THE JOURNAL OF BIOLOGICAL CHEMISTRY
Vol. 279, No. 41, Issue of October 8, pp. 43330–43335, 2004
Printed in U.S.A.
© 2004 by The American Society for Biochemistry and Molecular Biology, Inc.

Crystal Structure of CD26/Dipeptidyl-peptidase IV in Complex with Adenosine Deaminase Reveals a Highly Amphiphilic Interface*[S]

Received for publication, May 5, 2004, and in revised form, June 3, 2004
Published, JBC Papers in Press, June 22, 2004, DOI 10.1074/jbc.M405001200

Wilhelm A. Weihofen‡, Jiango Liu§, Werner Reutter§, Wolfram Saenger‡¶, and Hua Fan§‖

From the ‡Institut für Chemie/Kristallographie, Freie Universität Berlin, Takustrasse 6, D-14195 Berlin, Germany and the §Institut für Molekularbiologie und Biochemie, Charité-Universitätsmedizin Berlin, Arnimallee 22, D-14195 Berlin, Germany

Dipeptidyl-peptidase IV (DPPIV or CD26) is a homodimeric type II membrane glycoprotein in which the two monomers are subdivided into a β-propeller domain and an α/β-hydrolase domain. As dipeptidase, DPPIV modulates the activity of various biologically important peptides and, in addition, DPPIV acts as a receptor for adenosine deaminase (ADA), thereby mediating co-stimulatory signals in T-lymphocytes. The 3.0-Å resolution crystal structure of the complex formed between human DPPIV and bovine ADA presented here shows that each β-propeller domain of the DPPIV dimer binds one ADA. At the binding interface, two hydrophobic loops protruding from the β-propeller domain of DPPIV interact with two hydrophilic and heavily charged α-helices of ADA, giving rise to the highest percentage of charged residues involved in a protein-protein contact reported thus far. Additionally, four glycosides linked to Asn^{229} of DPPIV bind to ADA. In the crystal structure of porcine DPPIV, the observed tetramer formation was suggested to mediate epithelial and lymphocyte cell-cell adhesion. ADA binding to DPPIV could regulate this adhesion, as it would abolish tetramerization.

CD26 or dipeptidyl-peptidase IV (DPPIV,[1] EC 3.4.14.5) is a ubiquitous, multifunctional integral type II membrane glycoprotein located on the surface of a variety of epithelial, endothelial, and lymphoid cells, and it also occurs in soluble form in serum. As serine exopeptidase, DPPIV cleaves N-terminal dipeptides from polypeptides with proline or alanine preferentially in the penultimate position, thereby regulating the activity of a variety of biologically important peptides (1). Besides its peptidase activity, one of the main functions of DPPIV is binding to adenosine deaminase (ADA, EC 3.5.4.4) and to the extracellular matrix (2). All of these functions can influence T-cell proliferation (3, 4). In addition, DPPIV interacts with human immunodeficiency virus-1 Tat protein (5), and the human immunodeficiency virus envelope protein gp120 inhibits binding of DPPIV to ADA (6).

Crystal structures of DPPIV free and in complex with different inhibitors show that DPPIV is a "U"-shaped homodimer, the two monomers being related by a pseudo-2-fold rotation axis coinciding with the symmetry axis of the "U" (3, 7–9). The six-residue-long N-terminal cytoplasmic tails of the DPPIV dimer are followed by 22-residue-long transmembrane α-helices. The subsequent extracellular ectodomains are divided into two domains each. Eight-bladed β-propeller domains (Arg^{54}-Asn^{497}) form the arms of the "U" distal to the membrane plane, and α/β-hydrolase domains (Gln^{508}-Pro^{766}) proximal to the membrane form the bend of the "U" and harbor the catalytic triads that are required for peptidase activity.

Soluble DPPIV (without transmembrane α-helix) migrates as a dimer in gel filtration (3) but can also form higher molecular weight assemblies with apparent mass of 900 kDa (10). This could be due to a tetrameric assembly as observed in the crystal structure of porcine DPPIV (pDPPIV) that is associated with head-to-head binding between the ends of the arms of two "U"-shaped DPPIV dimers to form a "⊂ ⊃"-shaped complex. Engel *et al.* (9) suggested that pDPPIV tetramerization might be involved in cell-cell contacts, and this view would explain why DPPIV promotes adhesion between lymphocytes and epithelial cells that is inhibited by the addition of exogenous ADA (11).

ADA is a ubiquitous, soluble, and globular enzyme with a TIM barrel fold (eight parallel β-strands forming a barrel decorated by α-helices) (12). It is present in all mammalian tissues and involved in the development and function of lymphoid tissue. ADA binds specifically to the DPPIV of humans, cattle, and rabbits with dissociation constants of 3 to 20 nM depending on the organism (3). Binding of ADA to DPPIV is important in regulating the extracellular local concentration of adenosine (13, 14). Inhibition of ADA reduces signals mediated by CD3 and T-cell receptors and suggests a correlation between ADA binding to DPPIV and T-cell activation (15), as elevated adenosine concentration inhibits the proliferation of T-lymphocytes. Although they share high sequence homology with their higher mammal analogs, DPPIV and ADA of rodents do not form a complex.

A cryo-electron microscopy study of the DPPIV·ADA complex at 22 Å resolution confirmed the location of the ADA binding site on the β-propeller domain of DPPIV (16). Because details of intermolecular interactions remained elusive at this low resolution, ADA was oriented relative to DPPIV on the basis of

* These studies have been supported by DFG-Sonderforschungsbereich 449 and Fonds der Chemischen Industrie. The costs of publication of this article were defrayed in part by the payment of page charges. This article must therefore be hereby marked "*advertisement*" in accordance with 18 U.S.C. Section 1734 solely to indicate this fact.

[S] The on-line version of this article (available at http://www.jbc.org) contains a supplemental table.

The atomic coordinates and structure factors (code 1W1I) have been deposited in the Protein Data Bank, Research Collaboratory for Structural Bioinformatics, Rutgers University, New Brunswick, NJ (http://www.rcsb.org/).

¶ To whom correspondence may be addressed. Tel.: 49-30-838-53412; Fax: 49-30-838-56702; E-mail: saenger@chemie.fu-berlin.de.

‖ To whom correspondence may be addressed. Tel.: 49-30-8445-1544; Fax: 49-30-8445-1541; E-mail: hua.fan@charite.de.

[1] The abbreviations used are: DPPIV, dipeptidyl-peptidase IV; ADA, adenosine deaminase; hADA, human ADA; bADA, bovine ADA; mADA, murine ADA; hDPPIV, human DPPIV; pDPPIV, porcine DPPIV; rDPPIV, rabbit DPPIV; PDB, Protein Data Bank; r.m.s., root mean square; WT, wild type; TIM, triose-phosphate isomerase.

This paper is available on line at http://www.jbc.org

mutagenesis studies, which suggested that helix α2 of ADA binds to segments of β-propeller blades IV and V of DPPIV (17–19).

We crystallized the complex of human DPPIV (hDPPIV) ectodomain with bovine ADA (bADA), which shares 91% amino acid sequence homology with human ADA (hADA). The crystal structure determined at 3.0 Å resolution shows the intermolecular contacts in a highly amphiphilic interface that contribute to and stabilize hDPPIV·bADA complex formation.

TABLE I
Crystallographic data and refinement statistics

Space group	C2
Cell constants	a = 158.1 Å, b = 168.5 Å, c = 238.8 Å, β = 100.54°
Resolution range (Å)	30.0–3.03
Number of observations	229,245
Number of unique reflections	100,817
Completeness (%)[a]	85.3 (81.9)
$\langle I/\sigma(I)\rangle$[a]	8.4 (2.1)
R_{sym} (%)[a,b]	8.9 (44)
Refinement statistics	
Number of residues/atoms	4,386/35,904
R_{work}	22.8
R_{free}	25.9
r.m.s. deviations[c]	
Bond lengths (Å)	0.009
Bond angles (°)	1.39

[a] Values in parentheses refer to the outer resolution shell.
[b] $R_{sym} = (\Sigma\ |I_{hkl} - \langle I\rangle|)/(\Sigma I_{hkl})$, where I_{hkl} is the observed and $\langle I\rangle$ is the obtained average intensity from multiple observations of symmetry-related reflections.
[c] Computed with PROCHECK. r.m.s., root mean square.

EXPERIMENTAL PROCEDURES

Production, Purification, and Crystallization of hDPPIV·bADA—Full-length, enzymatically active hDPPIV was expressed in Sf9 cells and purified (20). N-terminal sequencing showed that residues 1–29 were uniformly truncated during purification. The hDPPIV·bADA complex was prepared by mixing hDPPIV and bADA (Sigma type VIII from calf intestinal mucosa) with a molar excess of bADA in 20 mM Tris, 500 mM NaCl, pH 8.0, and incubating at 4 °C overnight. The formed complex was analyzed by gel electrophoresis under nondenaturing conditions (20), purified by gel filtration on Superdex 200 10/30 (Amersham Biosciences) with 20 mM Tris-HCl, 150 mM NaCl, pH 8.0 (16), and concentrated to 7 mg/ml. For crystallization, a reduced factorial screen (Hampton Research) was set up using the vapor diffusion method. Crystals were obtained with 20–22% polyethylene glycol 3350, 200 mM NaCl, and 100 mM Tris-HCl, pH 8.0, and optimized by microseeding. Prior to data collection, the crystals were soaked in 25% polyethylene glycol 3350, 200 mM NaCl, 100 mM Tris, pH 8.0, supplemented with 20% glycerol, and cryo-cooled. Diffraction quality improved by annealing the crystal to room temperature twice for 3 s.

Structure Determination—X-ray data were collected at BESSY II, Berlin, Germany (Beamline BL1 of Free University, Berlin) and processed with DENZO and SCALEPACK (21); see Table I. The structure of hDPPIV·bADA was solved by a molecular replacement method with the program MOLREP (22) using glycoside-depleted hDPPIV as a partial search model (Protein Data Bank (PDB) code 1N1M), yielding two DPPIV dimers per asymmetric unit. Difference electron density clearly showed the presence of ADA molecules. Although an additional search using bADA (PDB code 1KRM) located four bADA molecules, the asymmetric unit is occupied by two $(hDPPIV{\cdot}bADA)_2$ complexes. Refinement was done using the REFMAC5 program (23) by applying four-fold noncrystallographic symmetry restraints to the protein chains but omitting the interface regions (24). Manual model building was done with the program O (25). Glycoside residues could be fitted to the electron density at eight of the expected nine *N*-glycosylation sites except for Asn^{685}. For statistics, see Table I. The figures of molecules were prepared with MolScript (26) and RASTER3D (27).

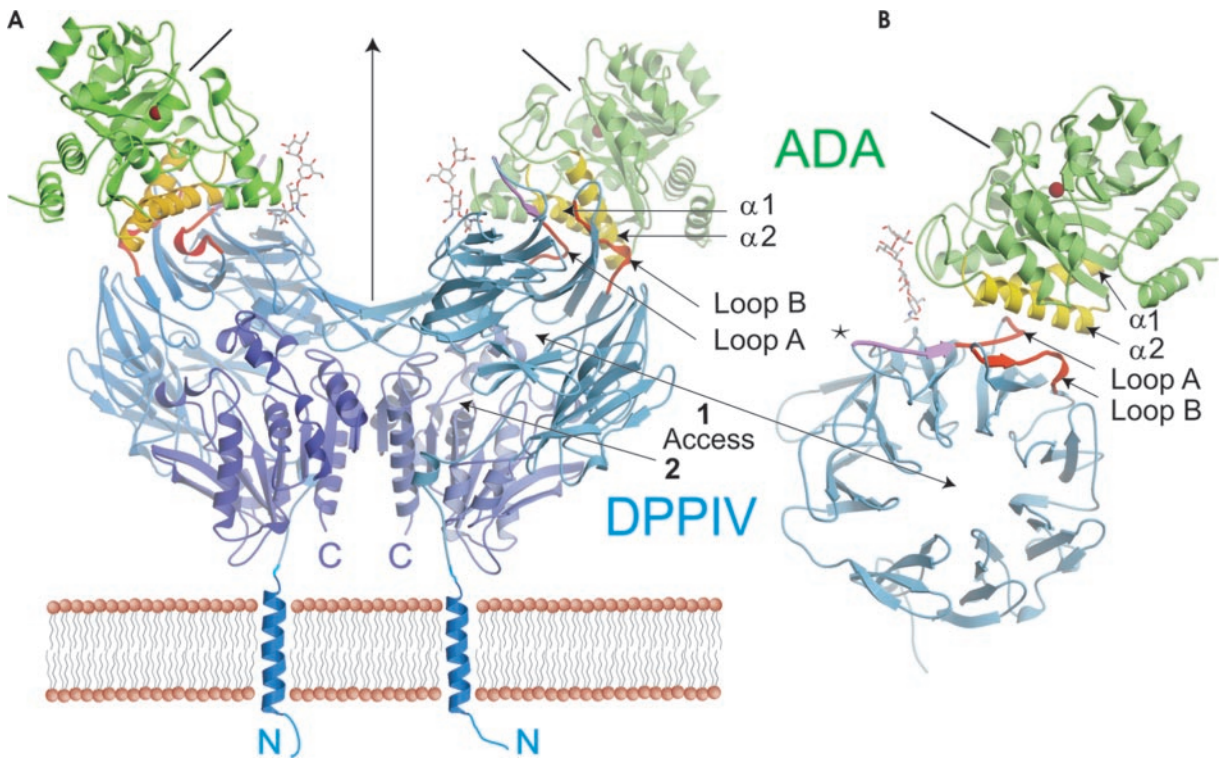

FIG. 1. **Overall structure ("U") of the $(hDPPIV{\cdot}bADA)_2$ complex.** *A*, the membrane and membrane anchor (not seen in the electron density) are drawn schematically. The view is normal to the pseudo-two-fold axis (*vertical arrow*) that relates the two hDPPIV·bADA units in $(hDPPIV{\cdot}bADA)_2$. The domains of hDPPIV are *violet* and *blue* for the α/β hydrolase and β-propeller domains, respectively; bADA is shown in *green*, active site Zn^{2+} is shown as a *red sphere*, and the oligosaccharide at conserved DPPIV-Asn^{229} is shown in *stick* representation. *Access arrow 1* points to the entrance of the substrate to the active site through the β-propeller, and *arrow 2* points through the side opening of hDPPIV. Orientations of the axes of the TIM barrels of bADA are represented by *black lines*. In the hDPPIV·bADA binding sites, loops A and B of hDPPIV are *red*, and α-helices α1 and α2 of bADA are *yellow*. *B*, view along the axis of the propeller domain of DPPIV, rotated by ~40° around the horizontal so that bADA moves toward the viewer. The *violet* β-strand N-terminal of loop A (*red*) is engaged in the tetramer formation of porcine DPPIV. The *asterisk* indicates the position of glycosylated Asn^{281}.

RESULTS AND DISCUSSION

Overall Structure—hDPPIV was expressed and purified as full-length protein, but N-terminal sequencing revealed that it was cleaved during purification after residue 29, explaining its solubility in detergent-free buffer. The final electron density map of hDPPIV·bADA featured no density for the N-terminal residues 30–38 presumably because of high flexibility and/or disorder of this segment. Ser^{39} is the first residue with appropriate electron density of the hDPPIV ectodomain.

The crystal asymmetric unit contains two complexes, each with $(hDPPIV{\cdot}bADA)_2$ stoichiometry and a molar mass of 275 kDa (Fig. 1*A*). Each hDPPIV binds one bADA at the periphery of the β-propeller domain near the ends of the arms of the "U" (Fig. 1*B*), thereby preserving the pseudo-two-fold symmetry of the complex (Fig. 1*A*). All crystal contacts of $(hDPPIV{:}bADA)_2$ are distant to the interface region, suggesting that they will not structurally influence the binding of hDPPIV to bADA. Superposition of main chain structures of hDPPIV (PDB code 1N1M) and bADA (PDB code 1KRM) with their equivalents in $(hDPPIV{\cdot}bADA)_2$ yielded average root mean square deviations of 0.8 and 0.9 Å, respectively, indicating that their structures are nearly identical. In particular, the interface regions of hDPPIV and bADA do not rearrange significantly upon complex formation and show root mean square deviations of 1.0 and 0.6 Å, respectively, for main chain atoms. In the $(hDPPIV{\cdot}bADA)_2$ complex, bADA does not block the possible path of substrate through the central tunnel of the β-propeller or through the side opening to the active site of hDPPIV (Fig. 1), and conversely, binding of hDPPIV (Fig. 1*B*) does not block the active site of bADA. This agrees with studies indicating that upon complex formation, DPPIV and ADA remain catalytically active (28).

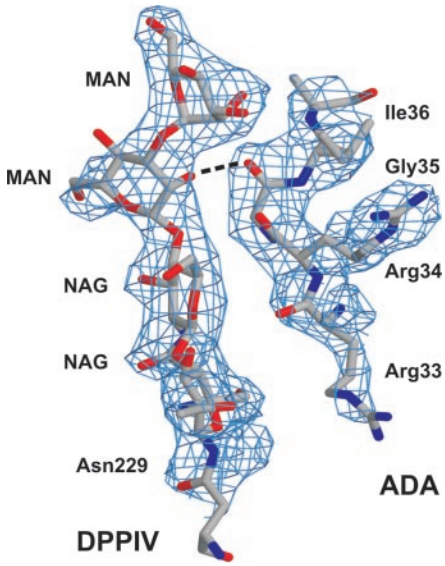

FIG. 2. **Glycoside residues bound to Asn^{229} of hDPPIV interact with ^{33}Arg-Arg-Gly-Ile^{36} of bADA.** Electron density is drawn at the 1.2 σ level. Carbon atoms are *gray*, oxygen is *red*, and nitrogen is *blue*. The *dashed black line* indicates a hydrogen bond ($Man_3O2H{:}Gly^{35O}$, 2.6 Å). *MAN*, mannose; *NAG*, *N*-acetylglucosamine.

The hDPPIV·bADA Interface—The hDPPIV:bADA interface buries 930-$Å^2$ solvent-accessible surface area/polypeptide corresponding to 3 and 7% of the total accessible surface of individual hDPPIV and bADA molecules, respectively. Four glycoside residues linked to the conserved Asn^{229} of hDPPIV are well defined in the electron density (Fig. 2). They contact ^{33}Arg-Arg-Gly-Ile^{36} of bADA and form one intermolecular hydrogen bond, and the protein-sugar interactions increase the buried surface by 170 $Å^2$. This contact, however, is not a prerequisite for ADA binding as shown by site-directed mutagenesis of $Asn^{229} \rightarrow$ Ala or deletion of any other *N*-glycosylation site (29).

hDPPIV binds bADA with two adjacent loops. Loop A (Ile^{287}-Asp^{297}) connects blades IV and V, and loop B (Asp^{331}-Gln^{344}) links β-strands β3 and β4 of blade V (Fig. 3). The loops protrude from the propeller blades and form a cleft accommodating helix α2 (Pro^{126}-Asp^{143}) of bADA (Fig. 4*A*). Interactions between helix α1 (Arg^{76}-Ala^{91}) of bADA and loop A of hDPPIV complete the interface (Fig. 4). As indicated in Fig. 3 by *triangles*, 14 and 13 residues in hDPPIV and bADA, respectively, are engaged in intermolecular contacts at the binding interface (see Fig. 4*B*). The supplementary information provides all interfacial contacts shorter than 3.9 Å.

A total of 11 intermolecular hydrogen bonds are formed between hDPPIV and bADA (Fig. 4). bADA-Glu^{139} on helix α2 appears to be important, as the carboxylate oxygen Oε1 forms hydrogen bonds to loop A of hDPPIV involving hDPPIV-Ala^{291}NH, hDPPIV-Ser^{292}NH, and hDPPIV-Ser^{292}Oγ. In addition, bADA-Glu^{139}Oε2 is hydrogen-bonded to hDPPIV-

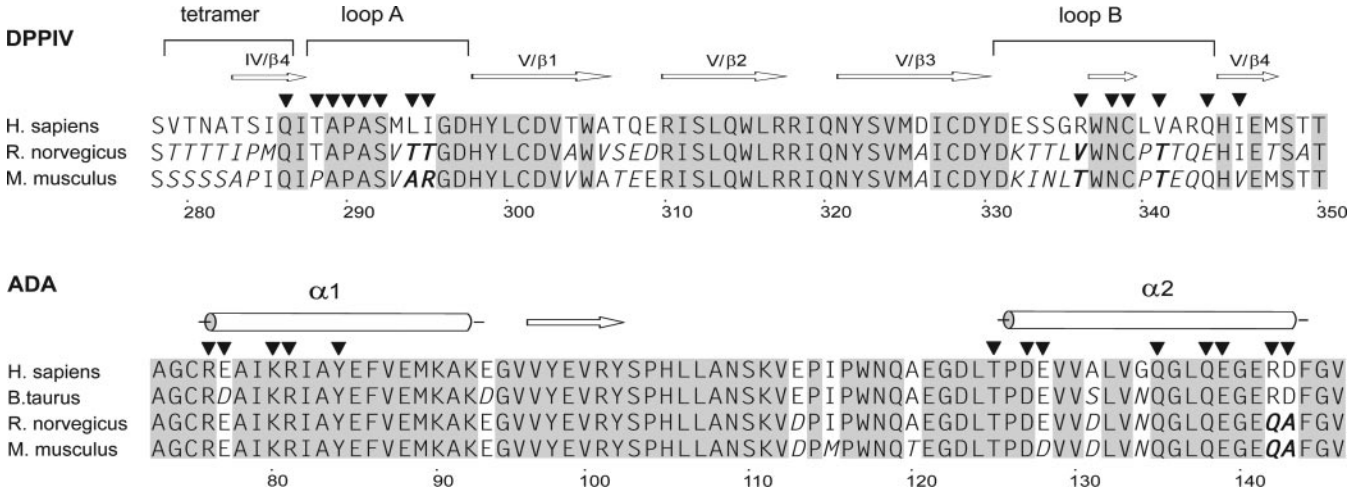

FIG. 3. **Amino acid sequence alignment of DPPIV and ADA binding segments.** *Black triangles* indicate amino acids engaged in complex formation. Identical and different amino acids are shown with *gray* and *white background*, respectively. Altered positions are in *italics*, and *letters* in *bold italic* denote nonconserved residues in rodents (*R. norvegicus, M. musculus*). *Top*, segment of human, rat, and mouse DPPIV with β-strands indicated by *arrows* labeled with β-propeller blades in *roman* and β-strands in *arabic numbers*, respectively. *Loop A* and *loop B* indicate segments of DPPIV engaged in hDPPIV·bADA complex formation and the *tetramer* segment is engaged in tetramer formation in porcine DPPIV. *Bottom*, segment of human, bovine, and rodent (rat and mouse) ADA binding to DPPIV. α-Helices are indicated and labeled as *α1* and *α2*.

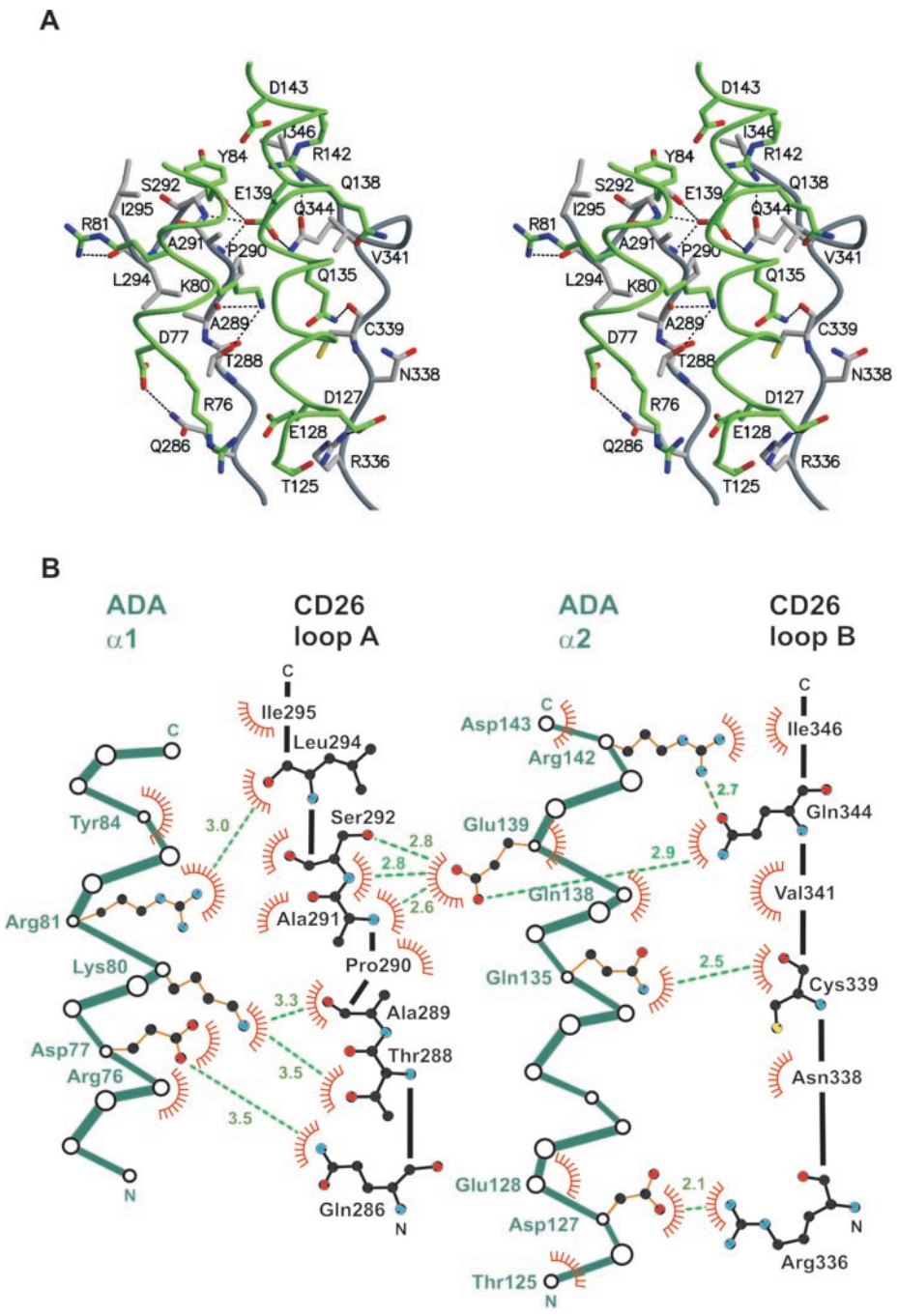

FIG. 4. **The interface between bADA and hDPPIV.** *A*, stereo plot of the hDPPIV·bADA interface, with bADA segments in *green* and hDPPIV segments in *gray*. Hydrogen bonds are indicated by *black dashed lines*. *B*, schematic representation of interactions between hDPPIV and bADA residues. Carbon atoms are shown in *black*, and nitrogen and oxygen atoms are as described in the legend to Fig. 2. Distances are in Å. Direct hydrogen bonds between proteins are shown as *green dashed lines*, and hydrophobic contacts are indicated by *red eyelashes*. This figure was partly generated with Ligplot (34).

Gln^{344}Nϵ on loop B, and hDPPIV-Gln^{344}Oϵ is in contact with bADA-Arg^{142}Nη on helix α2. The array of 11 hydrogen bonds with one hydrogen bond per 169 Å^2 of buried surface is in close agreement to the average value of 10 hydrogen bonds per protein-protein interface and one hydrogen bond per 170 Å^2 of buried interface area (30).

The interface in the hDPPIV·bADA complex is strongly amphiphilic. Of the 14 residues of hDPPIV forming intermolecular contacts at the interface, seven are apolar, six neutral polar, and only one (Arg^{336}) is charged (Figs. 3, 4*B*, and 5). This agrees grossly with the average distribution of residues in protein-protein interfaces, which comprise 57% apolar, 24% neutral polar, and 19% charged residues (30). By contrast, all of the 13 residues forming the interface region of bADA are polar, and among these, 9 (69%) are charged (see Fig. 5). The charged residues of bADA form two *intra*molecular and one *inter*molecular salt bridges (bADA-Arg^{76}···bADA-Glu^{128}, bADA·Arg^{142}···bADA-Asp^{143}), and (bADA-Asp^{127}···hDPPIV-Arg^{336}, respectively), and the other charged residues of bADA form hydrogen bonds to hDPPIV (Fig. 4). The highly charged interface region of bADA is unusual. Of all 27 residues participating in complex formation at the hDPPIV·bADA interface, 10 (37%) are charged, which is the highest percentage ever observed in protein·protein complexes, with the next highest value being 27% (30). As the sequences of human and bovine ADA are identical at the binding interface (Fig. 3), except for the conservative substitution hADA-Glu^{77}/bADA-Asp^{77} that forms a hydrogen bond to hDPPIV-Gln^{286}Nϵ (Fig. 4), structures of hDPPIV in complex with bovine and human ADA are supposed to be nearly identical.

Binding Studies Are Consistent with the (hDPPIV·bADA)$_2$ Structure—ADA from mouse and rat does not bind to endogenous DPPIV but binds weakly (in the μM range) to the DPPIV of primates, cattle, and rabbits. Although this lack of complex

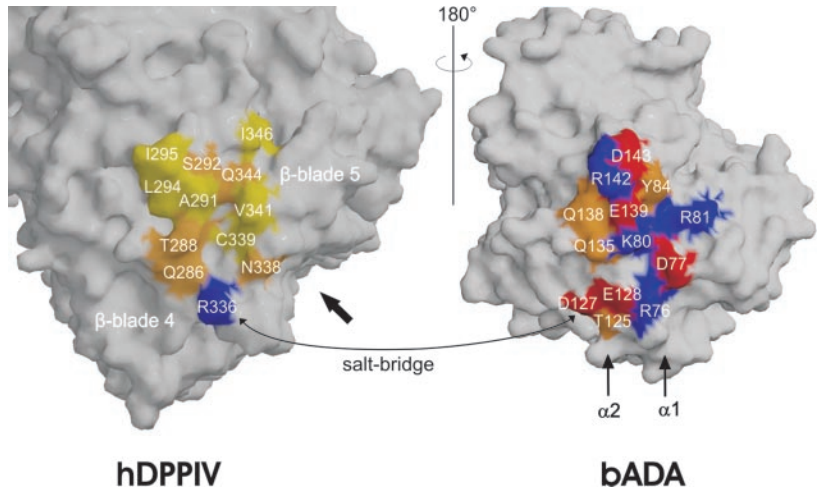

FIG. 5. **Surface representation of the hDPPIV·bADA interface**. This figure was drawn with GRASP (35). Contacting residues (distance cutoff, 3.9 Å) are assigned in one-letter code followed by sequence number. Positively and negatively charged residues are *blue* and *red*, unpolar and polar but uncharged residues are *yellow* and *orange*, respectively. The *bold arrow* indicates the access to the active site through the β-propeller opening of DPPIV and the *thin curved double arrow* indicates the salt bridge between hDDPIV-Arg^{336} and bADA-Asp^{127}. The two *parallel arrows* indicate the location and orientation of α-helices α1 and α2 of bADA as depicted in Figs. 1 and 3.

formation in rodents might be associated with amino acid substitutions in loops A and B of DPPIV and in helix α2 of ADA (Fig. 3), it has inspired mutational, binding, and kinetic studies on complex formation between DPPIV (18) and ADA (31).

For wild type (WT) hADA nearly all residues on helix α2 were substituted, and the binding of the variants to WT rabbit DPPIV (rDPPIV) was studied in terms of dissociation constants (K_D) and binding kinetics (k_{on}, k_{off}) (19). The affinity of the complex between WT hADA and rDPPIV (K_D = 17 nM) is ~300× stronger than between WT murine ADA (mADA) and rDPPIV (K_D = 5,400 nM). Compared with WT hADA, the most significant effects of single point mutations performed on helix α2 of hADA were found with Glu^{139} → Ala, Arg^{142} → Ala, and Asp^{143} → Ala, which showed an ~10- to 8-fold decrease in binding affinity to rDPPIV, with K_D between 160 and 112 nM (31). In all cases, the kinetic constants for complex formation (k_{on}) were comparable (k_{on} ~2×10^4 M^{-1} s^{-1}) and similar to that for WT hADA and rDPPIV, whereas those for complex dissociation differed by one power (k_{off} ~$2–4 \times 10^{-3}$ s^{-1}) compared with WT hADA, (k_{off} ~4×10^{-4} s^{-1}. Such behavior (nearly constant k_{on} but differing k_{off} in point-mutated protein complexes) suggests important contributions by hydrophobic interactions (32), which, besides the salt bridges and hydrogen bonds detailed above, must add considerably to hDPPIV·bADA binding. This agrees with the finding that the (hDPPIV·bADA)$_2$ complex dissociates at low ionic strength, suggesting that hydrophobic amino acids are essential for binding (33).

As interfacial residues of mADA and hADA differ solely in positions 142 and 143 on helix α2 (Fig. 3), a chimeric mADA construct containing the human α2 helix (residues 126–143) would be expected to bind to rDPPIV in a similar manner as WT hADA. The expected complex, however, showed a ~35-fold reduced K_D of 591 nM compared with ~17 nM for rDPPIV·hADA. This is not due to conformational changes of α2, as superimposed backbone atoms of helices α1 and α2 of free mADA (PDB code 2ADA) with (hDPPIV·bADA)$_2$ yielded a root mean square deviation of 0.53 Å. Although this is not significant at the 3.0-Å resolution level, the differences in dissociation constants may be due to other substitutions in mADA compared with hADA. The (hDPPIV:bADA)$_2$ model shows that two nonconserved residues in the binding region of bADA, Gln^{175} and Ser^{131}, are located at ~5 Å to Asn^{338} of hDPPIV and exchanged for charged Lys^{175} and Asp^{131} in mADA. This change could lead to far reaching electrostatic effects, thereby reducing the binding affinity in the complex formed by rDPPIV and chimeric mADA.

hDPPIV binds with a hydrophobic surface to ADA (Fig. 5). Compared with rodent DPPIV, which does not bind to endogenous ADA, four residues in the ADA binding site of hDPPIV are not conserved in any of the two rodent sequences, as depicted in Fig. 3. These are the bulky and hydrophobic residues Leu^{294}, Ile^{295}, and Val^{341} in hDPPIV that are all replaced by Thr in rat and by Ala^{294}, Arg^{295}, and Thr^{341} in mouse DPPIV, respectively. The positively charged Arg^{336} in hDPPIV is replaced by Val^{336} and Thr^{336} in rat and mouse, respectively. The significance of Leu^{294} or Val^{341} for ADA binding affinity was shown by mutational and subsequent binding studies, which indicated that mutations Leu^{294} → Ala or Val^{341} → Ala in hDPPIV reduced binding affinity to bADA, and drastic replacements Leu^{294} → Arg and Val^{341} → Lys even abolished bADA binding. The mutation Ile^{295} → Ser showed no detectable effect (18), probably because Ile^{295} is located at the outer interface region (Figs. 4 and 5). The introduction of these three bulky hydrophobic residues in hDPPIV increases the hydrophobicity of the interface (Fig. 5). This may indicate a directional shift to the evolution of strong ADA binding affinity to DPPIV in higher mammals contrasted to the loss of binding in rodents as proposed by Abbott *et al.* (18).

The fourth nonconserved residue in the ADA binding site of hDPPIV is Arg^{336}, which is replaced for Val and Thr in rat and mouse DPPIV, respectively (Fig. 3). Arg^{336}, the only charged residue in the hDPPIV interface, forms a salt bridge to bADA-Asp^{127} (see Figs. 4 and 5) and might therefore improve binding affinity.

ADA Binding Would Interfere with Tetramer Formation of DPPIV—Because the (hDPPIV·bADA)$_2$ complex does not show significant structural changes compared with the isolated components hDPPIV and bADA, and their enzymatic activities are not affected (28), any modulation of a DPPIV-mediated signal transduction across the membrane that is induced by ADA binding may consequently be associated with yet unidentified sterical interference.

In this context, porcine DPPIV is of interest because it shares 88% amino acid sequence identity with hDPPIV and crystallized as a tetramer forming a "⊂ ⊃"-shaped complex (9). This is associated with the four β-strands Asn^{279}–Gln^{286} that form two antiparallel β-sheets, thus extending the propeller blades IV to two eight-stranded β-sheets, and the dimer-dimer interactions are augmented by the outer β-strands of blades V (9). These segments (indicated by *violet arrows* in Fig. 1) share a homologous sequence in hDPPIV (Fig. 3), and although Gln^{286} is engaged in bADA binding (Fig. 4*B*), tetramer formation of DPPIV and binding of ADA are mutually exclusive. With this view, a recent study is explained that shows that hDPPIV promotes adhesion of lymphocytes to human epithelial cells, and that adhesion is significantly reduced by incubation with

exogenous ADA (11). This suggests that ADA could regulate cell-cell adhesion mediated by DPPIV, although no evidence has yet been provided that DPPIV directly participates in cell-cell adhesion.

The proposed key role of the glycosylation state of Asn^{279} in preventing or enabling ADA binding (9), however, can be ruled out. This is because $(hDPPIV{\cdot}bADA)_2$ shows electron density for two *N*-acetylglucosamine residues attached to each Asn^{281} (corresponding to Asn^{279} in the porcine sequence) at an ~15 Å distance to the bADA surface (indicated by an *asterisk* in Fig. 1*B*), which is too far to directly interfere with ADA binding.

Acknowledgments—We are grateful to Dr. Jörg Dobers for initial work, to Melanie Leddermann and Sabine Stehling for excellent technical assistance, to the staff at BESSY II (Berlin, Germany) for help with x-ray data collection, and to Dr. Timm Maier for help with structure determination. We are also grateful to Dr. Christoph Weise for N-terminal sequencing of DPPIV.

REFERENCES

1. Mentlein, R. (1999) *Regul. Pept.* **85,** 9–24
2. Hanski, C., Huhle, T., Gossrau, R., and Reutter, W. (1988) *Exp. Cell Res.* **178,** 64–72
3. Gorrell, M. D., Gysbers, V., and McCaughan, G. W. (2001) *Scand. J. Immunol.* **54,** 249–264
4. von Bonin, A., Huhn, J., and Fleischer, B. (1998) *Immunol. Rev.* **161,** 43–53
5. Gutheil, W. G., Subramanyam, M., Flentke, G. R., Sanford, D. G., Munoz, E., Huber, B. T., and Bachovchin, W. W. (1994) *Proc. Natl. Acad. Sci. U. S. A.* **91,** 6594–6598
6. Valenzuela, A., Blanco, J., Callebaut, C., Jacotot, E., Lluis, C., Hovanessian, A. G., and Franco, R. (1997) *J. Immunol.* **158,** 3721–3729
7. Rasmussen, H. B., Branner, S., Wiberg, F. C., and Wagtmann, N. (2003) *Nat. Struct. Biol.* **10,** 19–25
8. Thoma, R., Loffler, B., Stihle, M., Huber, W., Ruf, A., and Hennig, M. (2003) *Structure (Camb)* **11,** 947–959
9. Engel, M., Hoffmann, T., Wagner, L., Wermann, M., Heiser, U., Kiefersauer, R., Huber, R., Bode, W., Demuth, H. U., and Brandstetter, H. (2003) *Proc. Natl. Acad. Sci. U. S. A.* **100,** 5063–5068
10. Lambeir, A. M., Diaz Pereira, J. F., Chacon, P., Vermeulen, G., Heremans, K., Devreese, B., Van Beeumen, J., De Meester, I., and Scharpe, S. (1997) *Biochim. Biophys. Acta* **1340,** 215–226
11. Gines, S., Marino, M., Mallol, J., Canela, E. I., Morimoto, C., Callebaut, C., Hovanessian, A., Casado, V., Lluis, C., and Franco, R. (2002) *Biochem. J.* **361,** 203–209
12. Wilson, D. K., Rudolph, F. B., and Quiocho, F. A. (1991) *Science* **252,** 1278–1284
13. Kameoka, J., Tanaka, T., Nojima, Y., Schlossman, S. F., and Morimoto, C. (1993) *Science* **261,** 466–469
14. Schrader, W. P., West, C. A., Miczek, A. D., and Norton, E. K. (1990) *J. Biol. Chem.* **265,** 19312–19318
15. Martin, M., Huguet, J., Centelles, J. J., and Franco, R. (1995) *J. Immunol.* **155,** 4630–4643
16. Ludwig, K., Fan, H., Dobers, J., Berger, M., Reutter, W., and Bottcher, C. (2004) *Biochem. Biophys. Res. Commun.* **313,** 223–229
17. Dong, R. P., Tachibana, K., Hegen, M., Munakata, Y., Cho, D., Schlossman, S. F., and Morimoto, C. (1997) *J. Immunol.* **159,** 6070–6076
18. Abbott, C. A., McCaughan, G. W., Levy, M. T., Church, W. B., and Gorrell, M. D. (1999) *Eur. J. Biochem.* **266,** 798–810
19. Richard, E., Arredondo-Vega, F. X., Santisteban, I., Kelly, S. J., Patel, D. D., and Hershfield, M. S. (2000) *J. Exp. Med.* **192,** 1223–1236
20. Dobers, J., Zimmermann-Kordmann, M., Leddermann, M., Schewe, T., Reutter, W., and Fan, H. (2002) *Protein Expression Purif.* **25,** 527–532
21. Otwinowski, Z., and Minor, W. (1997) in *Macromolecular Crystallography Part A* (Carter, C. W., Jr., Sweet, R. M., eds) Vol. 276, pp. 307–326, Academic Press, New York
22. Vagin, A., and Teplyakov, A. (1997) *J. Appl. Crystallogr.* **30,** 1022–1025
23. Murshudov, G. N., Vagin, A. A., and Dodson, E. J. (1997) *Acta Crystallogr. Sect. D Biol. Crystallogr.* **53,** 240–255
24. CCP4. (1994) *Acta Crystallogr. Sect. D Biol. Crystallogr.* **50,** 760–763
25. Jones, T. A. (1978) *J. Appl. Crystallogr.* **11,** 268–272
26. Kraulis, P. J. (1991) *J. Appl. Crystallogr.* **24,** 946–950
27. Merritt, E. A., and Bacon, D. J. (1997) *Methods Enzymol.* **277,** 505–524
28. De Meester, I., Vanham, G., Kestens, L., Vanhoof, G., Bosmans, E., Gigase, P., and Scharpe, S. (1994) *Eur. J. Immunol.* **24,** 566–570
29. Aertgeerts, K., Ye, S., Shi, L., Prasad, S. G., Witmer, D., Chi, E., Sang, B. C., Wijnands, R. A., Webb, D. R., and Swanson, R. V. (2004) *Protein Sci.* **13,** 145–154
30. Lo Conte, L., Chothia, C., and Janin, J. (1999) *J. Mol. Biol.* **285,** 2177–2198
31. Richard, E., Alam, S. M., Arredondo-Vega, F. X., Patel, D. D., and Hershfield, M. S. (2002) *J. Biol. Chem.* **277,** 19720–19726
32. Murrell-Lagnado, R. D., and Aldrich, R. W. (1993) *J. Gen. Physiol.* **102,** 977–1003
33. Tsai, C. J., Lin, S. L., Wolfson, H. J., and Nussinov, R. (1997) *Protein Sci.* **6,** 53–64
34. Wallace, A. C., Laskowski, R. A., and Thornton, J. M. (1995) *Protein Eng.* **8,** 127–134
35. Nicholls, A., Sharp, K. A., and Honig, B. (1991) *Proteins* **11,** 281–296